

WHED: A Wearable Hand Exoskeleton for Natural, High-Quality Demonstration Collection

Mingzhang Zhu^{1*}, Alvin Zhu^{2,3*}, Jose Victor S. H. Ramos¹, Beom Jun Kim¹, Yike Shi^{2,3}, Yufeng Wu¹, Ruochen Hou¹, Quanyou Wang¹, Eric Song^{2,3}, Tony Fan³, Yuchen Cui², and Dennis W. Hong¹

Abstract—Scalable learning of dexterous manipulation remains bottlenecked by the difficulty of collecting natural, high-fidelity human demonstrations of multi-finger hands due to occlusion, complex hand kinematics, and contact-rich interactions. We present WHED, a wearable hand-exoskeleton system designed for in-the-wild demonstration capture, guided by two principles: wearability-first operation for extended use and a pose-tolerant, free-to-move thumb coupling that preserves natural thumb behaviors while maintaining a consistent mapping to the target robot thumb degrees of freedom. WHED integrates a linkage-driven finger interface with passive fit accommodation, a modified passive hand with robust proprioceptive sensing, and an onboard sensing/power module. We also provide an end-to-end data pipeline that synchronizes joint encoders, AR-based end-effector pose, and wrist-mounted visual observations, and supports post-processing for time alignment and replay. We demonstrate feasibility on representative grasping and manipulation sequences spanning precision pinch and full-hand enclosure grasps, and show qualitative consistency between collected demonstrations and replayed executions.

I. INTRODUCTION

Learning robust dexterous manipulation remains fundamentally bottlenecked by the availability of scalable, high-fidelity demonstrations that capture the closed-loop, contact-rich strategies humans use in daily life. While recent progress in robot learning has yielded strong returns from larger and more diverse human data, collecting such data for multi-finger hands is particularly challenging due to high-dimensional kinematics, frequent occlusion, and complex hand-object contact dynamics [1]–[4]. In contrast to parallel-jaw grippers, where portable teaching interfaces already scale well [5], high-DoF hands still rely heavily on interfaces that trade off naturalness, wearability, and motion fidelity—especially regarding the thumb, whose abduction/adduction and opposition are central to human dexterity.

Common sources of dexterous demonstrations fall into three categories: (i) **simulation/videos**, (ii) **robot teleoperation**, and (iii) **wearable interfaces** (gloves/exoskeletons). Video and simulation data can scale cheaply and broadly [6]–[9]; however, faithfully capturing contact forces, fine hand object interactions, and transferring them to hardware—remains challenging [9], [10]. Teleoperation yields demonstrations directly in the robot’s control space [11], [12], yet dexterous

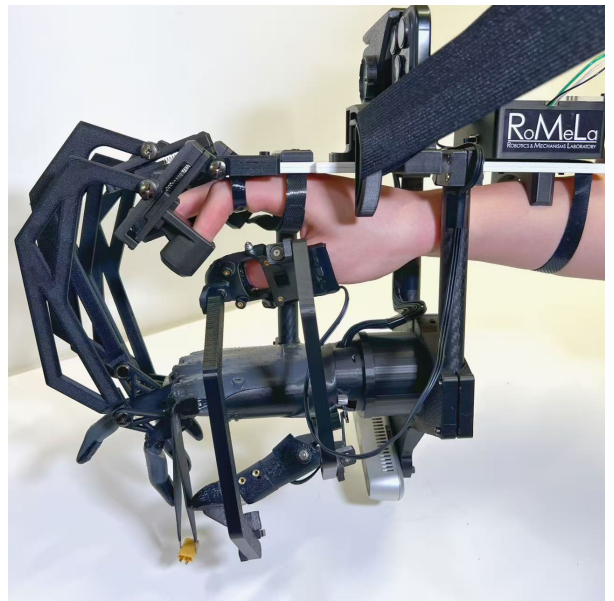


Fig. 1. A demonstration of a user picking up tweezers and using it to grasp an XT-30 connector.

hand teleoperation is often slow, unintuitive, expensive to scale, and limited by insufficient haptic feedback for contact-rich behaviors [11]. Wearable devices improve embodiment by mechanically coupling human motion to the robot, reducing retargeting ambiguity and enabling more natural demonstrations [13]–[15]. Nevertheless, these devices frequently trade comfort for fidelity and are difficult to fit across users due to anthropometric variation [16], [17].

Motivated by these gaps, we present WHED, a wearable hand-exoskeleton data-collection system designed around two principles: **wearability-first** and a **free-to-move thumb**. This approach preserves natural thumb behaviors during demonstration collection while maintaining a consistent, learnable mapping to the target robot thumb. Our design targets the practical regime where operators can perform long-horizon tasks in versatile environments with minimal setup, while retaining the motion fidelity needed for contact-rich dexterous learning [14], [15], [18]. In summary, our contributions are:

- A wearability-first hand exoskeleton architecture emphasizing comfort, adaptability, and robust use over extended data collection sessions.
- A free-to-move thumb mechanism that preserves the nat-

¹Department of Mechanical and Aerospace Engineering, UCLA, Los Angeles, CA, USA.

²Department of Computer Science, UCLA, Los Angeles, CA, USA.

³Department of Electrical Engineering, UCLA, Los Angeles, CA, USA.

*Denotes equal contribution.

ural thumb workspace while enabling a reliable mapping to robot thumb DOFs.

- A complete demonstration-collection pipeline for gathering natural, high-quality dexterous data.

II. RELATED WORK

A. Teleoperation for Dexterous Manipulation

While teleoperation is the primary method for collecting high-quality demonstrations, existing interfaces face distinct trade-offs. Vision-based systems offer an unencumbered experience but are fundamentally limited by line-of-sight occlusion and tracking instability during complex contact [6], [11]. Data gloves resolve these tracking issues and can provide force data [19], but they suffer from the "correspondence problem" [20]. Without physical constraints to enforce robot kinematics on the human hand, glove-based demonstrations often produce trajectories that are kinematically infeasible for the target hardware, despite recent algorithmic improvements in retargeting [21], [22].

B. Learning from Human Hand Videos

To bypass the hardware bottlenecks of teleoperation, recent research has pivoted toward learning directly from large-scale human videos [6], [7], [23]. These approaches leverage the massive scale of internet data to learn strong geometric and visual priors for hand-object interaction [24], [25]. However, video-based learning suffers from a "physicality gap": it lacks explicit information about contact forces and precise closed-loop dynamics [9], [10]. Consequently, policies learned purely from video often struggle to transfer to real-world robots without fine-tuning on contact-rich data collected via teleoperation [1], [26].

C. Exoskeleton and Mechanically Coupled Interfaces

Exoskeleton and mechanically coupled interfaces seek to reduce the embodiment gap by physically linking human motion to robot kinematics, often improving controllability relative to other methods [15], [18]. Recent systems such as **DexUMI** [13] aim to scale in-the-wild collection by pairing a lightweight wearable structure with vision-based reconstruction, but residual kinematic mismatch can induce rapid discomfort, limiting session duration. Similarly, devices such as **DexOP** [14] employ a linkage-driven passive hand interface to capture high-quality demonstrations by enforcing strong correspondence between the operator and the robot kinematics; however, these constraints can reduce cross-user adaptability (due to anthropometric variation) and restrict the natural thumb workspace required for complex in-hand manipulation [16], [17], [27]. In contrast, our system targets the missing intersection of wearability-first extended use and robust mapping, enabled by a free-to-move thumb that preserves natural thumb behaviors without sacrificing controllability.

III. HARDWARE DESIGN

A. Hardware Overview

WHED comprises (i) a linkage-driven wearable exoskeleton, (ii) a passive data-capture hand, and (iii) a self-contained sensing and power module for in-the-wild operation. The passive hand follows the geometry and aesthetics of the 6-DoF OYMotion ROH-AP001, featuring a 2-DoF thumb (IP flexion/extension and TM abduction/adduction) and single-DoF flexion for each of the four fingers. The exoskeleton mechanically couples the operator's motion to the passive hand via two architectures as shown in Fig. 2. The four fingers are connected through a linkage mechanism that provides near one-to-one correspondence in flexion/extension while accommodating inter-user kinematic variation, and the thumb is coupled through a multi-DOF interface that preserves the operator's natural thumb workspace. This design allows the exoskeleton thumb structure to translate and rotate relative to the palm while still transferring the key thumb degrees of freedom to the passive hand, improving comfort and fit across different hand sizes. A self-powered electronics box mounted on the dorsal side supplies onboard power and logging for extended, untethered data collection sessions.

B. Passive Hand Modification

To resolve the control ambiguity of the proprietary under-actuated thumb, we conducted a kinematic identification process to decouple its internal joint dependencies. We analyzed the relative joint motions using a URDF simulation, which served as the kinematic reference for our mechanical reverse engineering. Based on this analysis, a custom linkage-slide hybrid mechanism was implemented for the exoskeleton. This design minimizes the kinematic discrepancy between the passive hand and the target robot, ensuring that the recorded trajectories are physically feasible and directly executable on the real hardware.

To guarantee high-fidelity proprioceptive data acquisition, we engineered a rigid sensor mounting interface incorporating six joint encoders. A primary challenge in handheld teleoperation devices is signal noise induced by sensor misalignment during dynamic manipulation. We mitigated this by designing custom brackets reinforced with alignment ribs to constrain the encoder housing. This architecture prevents mechanical backlash and sensor detachment, thereby ensuring consistent measured joint-angle data under rapid motion.

C. Thumb Linkage

Thumb motion varies significantly across users and involves coupled base movements, making rigid joint-axis alignment uncomfortable and workspace-limiting in wearable exoskeletons. WHED adopts a pose-tolerant thumb interface that prioritizes wearability while preserving the two key passive-thumb DoFs for natural demonstrations: IP flexion/extension (J_2) and TM ab/ad (J_4).

As shown in Fig. 4 (a), the exoskeleton thumb includes an instrumented IP joint J_1 (angle ϕ) and connects to the

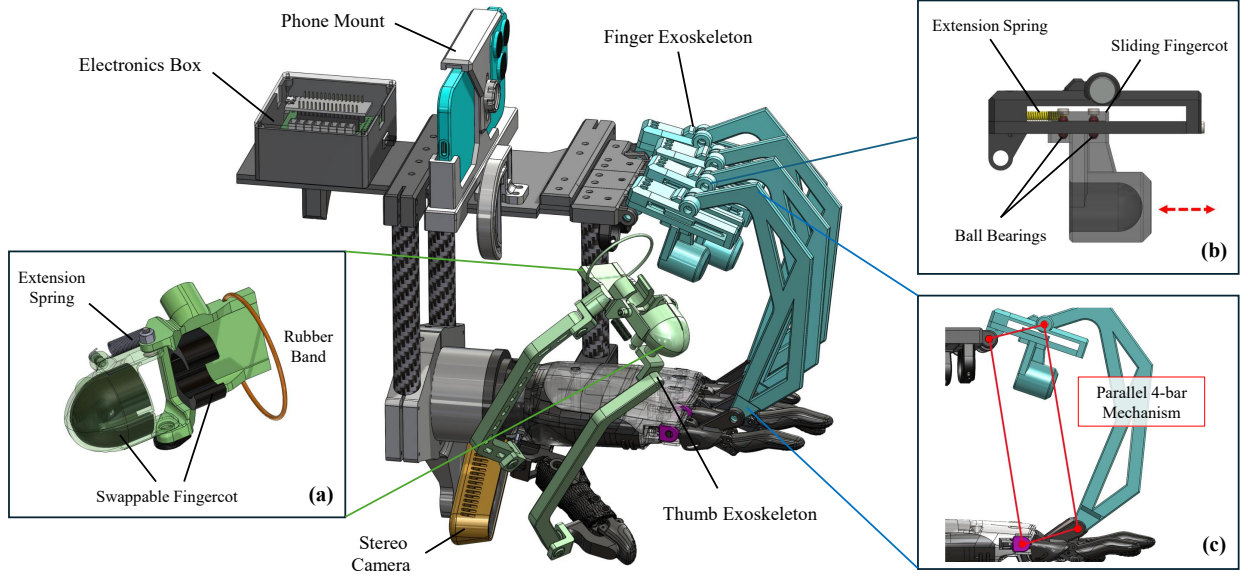


Fig. 2. Mechanical overview of WHED. WHED integrates a linkage-driven wearable exoskeleton, a passive data-capture hand, and an onboard sensing/power module. Insets highlight key subsystems: (a) pose-tolerant thumb coupling interface, (b) passive finger slider for cross-user fit, and (c) parallel four-bar finger linkage for motion transmission.

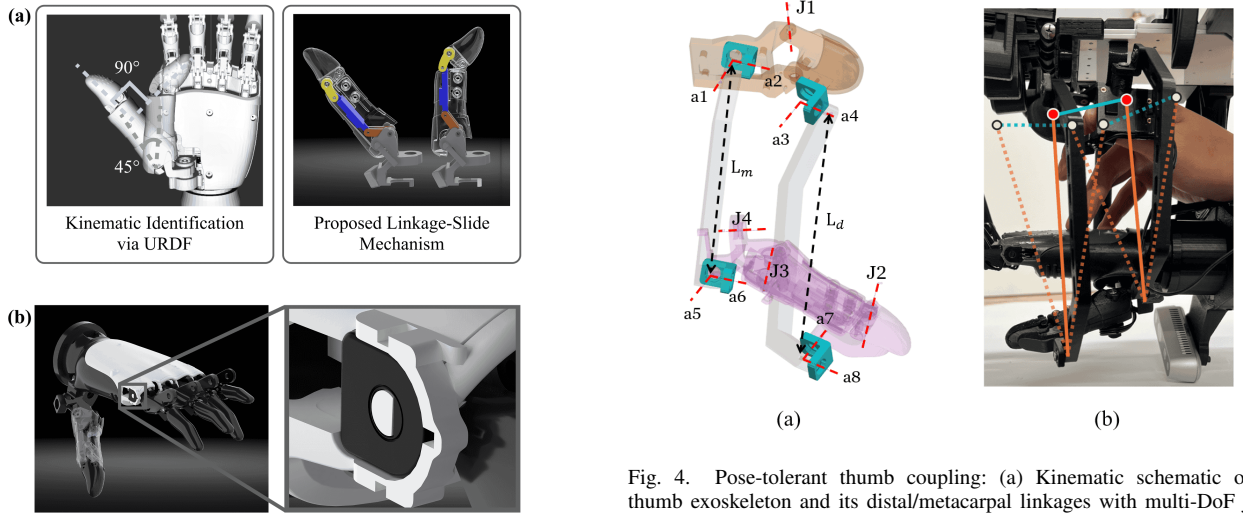


Fig. 4. Pose-tolerant thumb coupling: (a) Kinematic schematic of the thumb exoskeleton and its distal/metacarpal linkages with multi-DoF joints (a_1 – a_8). (b) Example “wobble space” during which the exoskeleton body can translate/rotate relative to the palm while the passive thumb posture remains unchanged.

Fig. 3. Passive-hand modification for kinematic executability and robust sensing. (a) URDF-based kinematic identification of the underactuated thumb informs a linkage–slider mechanism that decouples and reproduces the intended thumb DOFs. (b) Rigid encoder mounting with alignment ribs suppresses backlash-induced noise during dynamic operation.

passive thumb via two rigid linkages (distal and metacarpal). Each linkage terminates in multi-DoF rotational joints (a_1 – a_8), allowing the linkage endpoints to swivel and self-align. Consequently, the exoskeleton thumb body is not rigidly constrained to the palm and can translate/rotate relative to the hand while remaining mechanically coupled.

We describe this behavior with a lightweight constraint

model. Let ${}^B T_E \in SE(3)$ denote the exoskeleton pose relative to the palm base (Fig. 4). With linkage lengths L_d and L_m , and attachment points on the passive thumb ${}^B r_d(q_p), {}^B r_m(q_p)$ (from the passive-hand kinematics $q_p = [\theta_2 \ \theta_4]^T$), the coupling is characterized by two fixed-length constraints:

$$\|r_d^E - r_d(q_p)\| = L_d, \quad \|r_m^E - r_m(q_p)\| = L_m, \quad (1)$$

where r_d^E, r_m^E are the corresponding exos-side attachment points expressed in the palm frame via ${}^B T_E$. Because the linkage ends can freely rotate, these constraints primarily en-

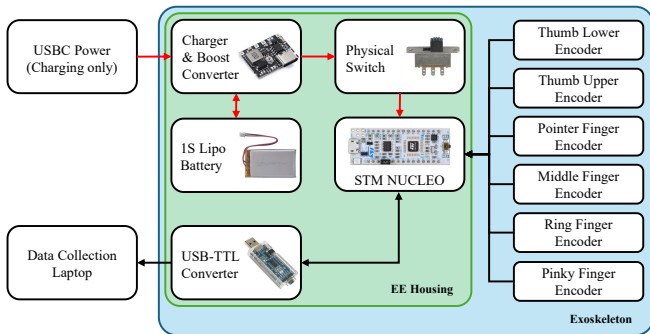


Fig. 5. Electronic system overview of the exoskeleton.

force distances rather than orientations, enabling the intended “free-to-move” self-alignment.

The design provides two complementary motion channels: J_1 transfers IP motion to J_2 , while the remaining relative pose change of the exoskeleton (captured by ${}^B T_E$) accommodates TM ab/ad at J_4 without strict alignment. Fig. 4 (b) shows “wobble-space” configurations, which are the allowable exoskeleton-body pose variations that maintain the passive-thumb posture. This ensures comfort and improves fit across users.

D. Finger Linkage

The wearable finger linkage is designed to map human finger motion to the data capture hand. A parallel four-bar linkage mechanism is employed to provide a near one-to-one kinematic correspondence between the operator’s MCP flexion and the passive finger flexion DoF. This direct mechanical mapping avoids extra linkages or tendons that might interfere with the machine learning pipeline used later on. To accommodate kinematic mismatch between the rigid linkage and the motion of the human finger, a passive slider mechanism is integrated into the finger linkage. The user inserts their finger into a sliding finger cup, which translates along a guided track with the aid of sliding ball bearings. This sliding degree of freedom allows for improved comfort and wearability as the mechanism can adapt to variations in finger length and joint trajectories across users. An extension spring is connected to the sliding finger cup toward the back end of the track, which ensures that the wearer’s fingertip remains fully seated within the finger cup throughout motion, guaranteeing reliable kinematic mapping.

E. Wearability Attachment

Mounting auxiliary sensors (e.g., stereo camera and phone) increases distal mass and can accelerate operator fatigue during extended data collection. To reduce this load without restricting motion, we integrate a passive support attachment as shown in Fig. 6(a) that provides gravity compensation via an elastic band routed over a curved guide. As the arm posture changes, the band slides along the guide to maintain a smooth force direction and an approximately consistent moment arm about the upper-limb joints, reducing parasitic

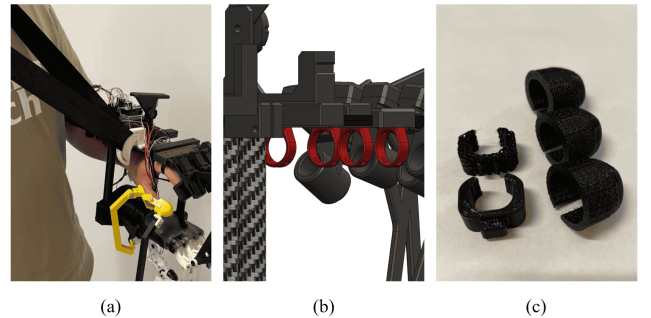


Fig. 6. Wearability and fit enhancements. (a) Curved guidance surface with an elastic band that provides passive gravity compensation while allowing arm motion. (b) Finger ring interface that stabilizes the linkage on the operator’s finger. (c) Swappable thumbcots and thumb holders that accommodate different thumb sizes and improve contact comfort.

shear and torsional loading. To further improve comfort and stability at the human–device interface, a finger-ring support shown in Fig. 6(b) constrains lateral motion of the finger linkage and reduces unintended forces applied at the fingertip. Finally, swappable thumbcots and thumb holders shown in Fig. 6(c) enable rapid resizing across users, improving fit and reducing localized pressure during long sessions.

F. Electronics

As shown in Fig. 5, the overall electronic system consists primarily of off-the-shelf components to maximize reproducibility. Power is supplied by a 1S LiPo battery with a module that supports periodic charging and regulates the supply to a stable 5V for the STM32F042 NUCLEO microcontroller (MCU). The MCU acquires analog voltage signals from the joint encoders (RDC506018A rotary sensors) mounted within the passive hand, and streams the joint angle information to a data collection laptop via a TTL-to-USB converter. A prototyping board was used to organize the wired connections and to keep all electronic components contained within a compact enclosure, while still allowing for servicing and future upgrades.

IV. DATA COLLECTION PIPELINE

A. Data Collection

1) *Finger Position Data*: Finger joint positions are collected using six analog encoders embedded in the exoskeleton’s kinematic structure. Each encoder is powered by a 3.3V supply voltage and outputs an analog voltage proportional to its angular position over the 0-3.3V range. These voltages are sampled by the 12-bit ADC integrated in the STM32F042 MCU. To achieve the 1 kHz sampling frequency, the system clock is set to 48 MHz, and the UART baud rate is configured to 460,800 bps. To minimize the CPU overhead during data transfer, we configure the ADC in Direct Memory Access mode to ensure non-blocking data communication.

A custom binary communication protocol is implemented for the serial communication between the MCU and the host side computer: each frame consists of a 2-byte header (0xAA,

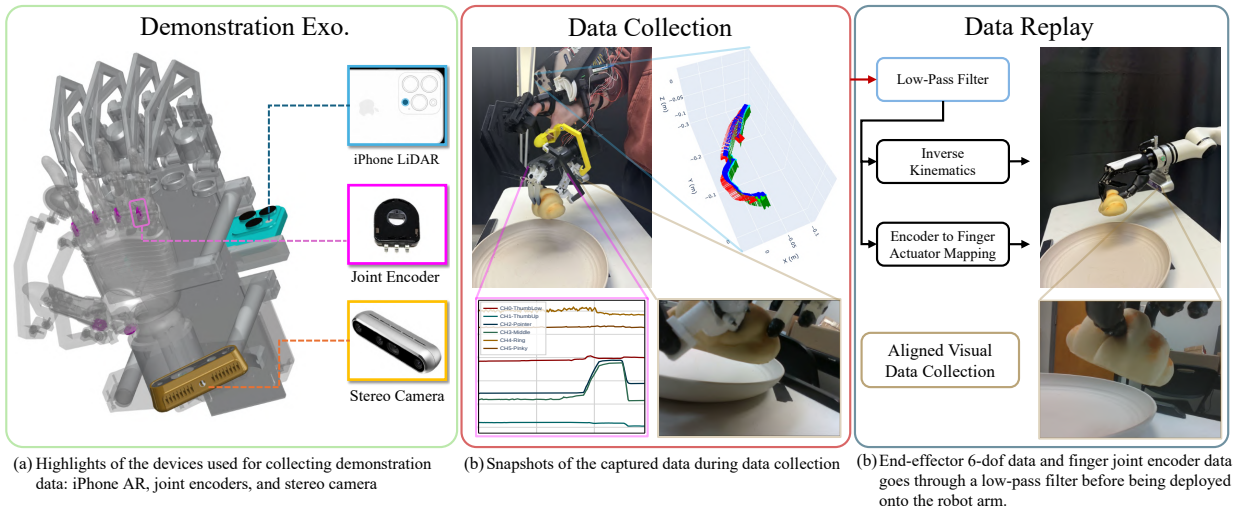


Fig. 7. An overview of the full demonstration exoskeleton, data collection, and data replay pipeline.

0xBB) followed by a 12-byte payload containing the raw ADC values for the six channels. Each 12-bit sample from the encoders is stored as a 16-bit unsigned integer, occupying 2 bytes in the payload. On the host side, a Python script parses the incoming binary stream, and timestamps each received frame using the host side hardware performance counter (`time.perf_counter_ns`). The script logs these raw sensor values ($d \in [0, 4095]$) and relative timestamps directly to a CSV file.

2) *End-Effector Pose*: The 6-DOF end-effector pose is captured using augmented reality (AR) tracking from an iPhone mounted as shown in Fig. 7a via the TeleDex application [28]. TeleDex leverages Apple’s ARKit framework for high-precision pose estimation, enabling smooth trajectories as illustrated in Fig. 7b. The application streams pose data at approximately 100 Hz over a network connection to the host computer, which buffers and resamples the data at a fixed rate of 60 Hz to ensure consistent timing and mitigate network jitter. Each sample consists of a 3D position vector (in meters), a unit quaternion representing orientation, and high-resolution nanosecond timestamps for temporal synchronization with other sensor modalities.

The dual-rate buffering strategy decouples network reception from data recording, ensuring robust operation during transient network interruptions. All samples are buffered in memory and written to CSV after collection completes, eliminating I/O latency from the sampling path. The system achieves sampling rates within 0.3 Hz of the target 60 Hz with period standard deviation below 4 ms.

3) *Visual Observation*: An Intel RealSense camera is mounted to the WHED wrist to capture visual observations (640×480 resolution at 30 Hz). It provides critical information regarding the hand’s relative pose with respect to task-relevant objects. Each frame is recorded with an associated timestamp.

B. Post Processing

1) *Time Synchronization*: To facilitate precise temporal synchronization with all data we collected, we use a synchronization pipeline. Data streams are aligned using 30 Hz video timestamps as the master reference. A nearest-neighbor search matches asynchronous encoder and pose data, discarding any matches with a temporal offset exceeding 70 ms.

2) *Filtering*: There exists high-frequency noise and intermittent signal spikes in the 1 kHz encoder data. To suppress this, we utilize a two-stage filtering process. First, a second-order Butterworth low-pass filter in Fig 7c with a cutoff frequency of 10 Hz is applied to remove electrical noise. Second, we implement a moving-average filter using a 30-sample window to further smooth transient outliers. This combined approach is similarly applied to the 6D end-effector pose data, ensuring jitter-free trajectories for the replay pipeline.

3) *Frame Transformation*: The raw pose data collected via iPhone LiDAR represents the motion of the smartphone rather than the hand’s end-effector. To resolve this kinematic discrepancy, we apply a rigid-body transformation $T_{EEF}^{Phone} \in SE(3)$ to map the phone’s coordinate frame into the EEf frame. This transformation accounts for the fixed spatial offset (translation and rotation) introduced by the phone mount. The corrected pose is then transformed into the global palm-base frame, ensuring that all 6D pose trajectories are consistently aligned with the robot’s operational space.

C. Data Replay

The data replay pipeline utilizes the synchronized and filtered data streams to command the robotic platform as shown in Fig 7c. To map human kinematics to the robot hand, we first calibrate the finger encoders by identifying the sensor values corresponding to the “fully open” and “fully closed” states for each channel. These raw readings are then converted into 16-bit motor control signals (0–65,535) via linear interpolation. A manually tuned gain is applied to this

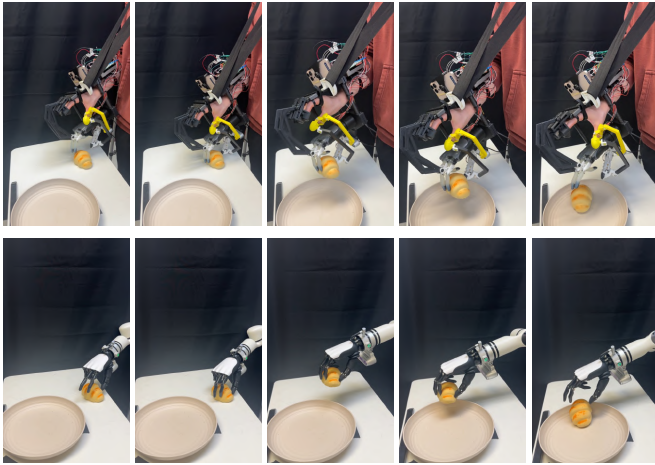


Fig. 8. Data collection and replay comparisons.

mapping to ensure responsive and natural finger movement during execution.

Arm trajectories are reconstructed by defining a static base pose P_{base} in the robot’s operational space. Because the action data is recorded as relative offsets, the absolute target pose P_{target} for each frame is calculated by adding the cumulative action vector to P_{base} . To maintain kinematic feasibility, all rotational components are wrapped within the $[-\pi, \pi]$ range. These synchronized hand and arm commands are then streamed to the hardware to execute the task.

V. RESULTS

A. Capable Tasks Demonstration

We performed demonstration experiments involving object pickup and placement into a container using four representative objects in the following order: an orange, a USB stick, a dry-erase marker, and a water bottle. Fig. 9 presents time-series snapshots of each task sequence, illustrating the progression from approach to grasp, lift, transport, and release. Each object highlights a distinct manipulation capability of the exoskeleton hardware. The orange demonstrates stable grasping of a curved, moderately compliant object, requiring distributed contact and smooth force modulation. The USB stick, due to its small size, emphasizes fine fingertip precision and accurate alignment to achieve a reliable pinch grasp. The dry-erase marker introduces a more challenging condition because of its slender geometry and slippery surface, requiring careful grip force regulation and stable orientation control to prevent slip during transport.

The final task with the water bottle highlights full-hand power grasping and the structural advantage of our pseudo-hand design. Unlike fingertip-only interfaces, the exoskeleton enables grasps that incorporate palm contact, allowing enclosure-style grasps around larger objects and improved load distribution across the hand. This expanded contact area increases grasp robustness and stability during lifting and placement. In contrast, methods such as [13], which lack

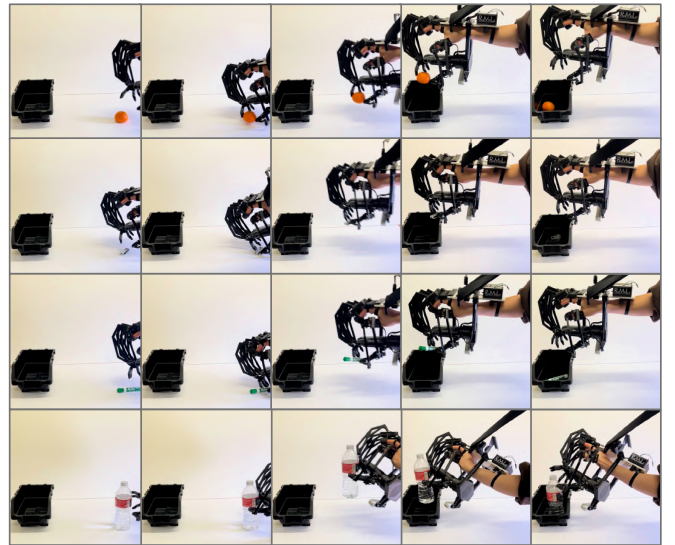


Fig. 9. Demonstration capability experiments on an orange, USB stick, dry-erase marker, and water bottle.

an integrated palm structure, are largely limited to fingertip-based grasps and cannot exploit palm-assisted stabilization. Collectively, these demonstrations show that the hardware supports a spectrum of manipulation strategies, ranging from high-precision pinch grasps to robust full-hand enclosure grasps, across objects with varying sizes, shapes, and surface properties.

B. Data Accuracy Validation

To assess the fidelity of the collected dataset, we executed a replay validation using the pipeline illustrated in Fig. 7c. When initialized from a fixed base configuration, the robot’s end-effector trajectories exhibited a high degree of kinematic similarity to the operator’s original motions. This correspondence, observed in both spatial translation and rotation, confirms that the retargeting and synchronization processes preserve the subtle dynamics of the demonstration.

As shown in Fig. 8, the replay trajectory during the approach and transport phases closely mirrors the demonstration, validating the accuracy of the smartphone-based LiDAR pose estimation and frame transformation. Furthermore, the robot achieved a stable grasp with an orientation matching the operator’s, indicating that the post-processed finger data accurately captures the intended grasp strategy. Finally, the object was released at a location nearly identical to the demonstration target, suggesting negligible error accumulation throughout the pipeline. Qualitatively, this ability to replicate complex, contact-rich tasks with minimal deviation demonstrates that data collected via WHED is both high-quality and reproducible.

VI. CONCLUSION

In this paper we present WHED, a wearable hand-exoskeleton system for collecting natural, high-quality ma-

nipulation demonstrations. WHED combines a wearability-first architecture with a pose-tolerant, free-to-move thumb coupling, a linkage-driven finger interface with passive fit accommodation, and onboard sensing for synchronized joint, pose, and visual data. We demonstrated end-to-end feasibility on representative grasping and manipulation sequences, including precision pinch and full-hand enclosure grasps. Detailed quantitative kinematic modeling, workspace/singularity analysis, and controlled user studies will be reported in our follow-up submission.

REFERENCES

- [1] Q. Ye *et al.*, “Visual-tactile pretraining and online multitask learning for dexterous manipulation,” *Science Robotics*, 2026.
- [2] Y. Liu, Y. Yang, Y. Wang *et al.*, “Realdex: Towards human-like grasping for robotic dexterous hand,” in *Proceedings of the International Joint Conference on Artificial Intelligence (IJCAI)*, 2024.
- [3] Y. Huang *et al.*, “Human-like dexterous manipulation for anthropomorphic five-fingered hands: A focused review,” *Elsevier Robotics and Autonomous Systems*, 2025, review Article.
- [4] E. Welte *et al.*, “Interactive imitation learning for dexterous robotic manipulation,” *PNAS Nexus*, 2025, under Review.
- [5] C. Chi, Z. Xu, C. Pan, B. Cousineau, Eric andich, and S. Song, “Universal manipulation interface: In-the-wild robot teaching without in-the-wild robots,” in *Robotics: Science and Systems (RSS)*, 2024.
- [6] K. Shaw *et al.*, “Learning dexterity from human hand motion in internet videos,” *arXiv preprint*, 2024.
- [7] H. G. Singh, A. Loquercio, C. Sferrazza, J. Wu, H. Qi, P. Abbeel, and J. Malik, “Hand-object interaction pretraining from videos,” 2024.
- [8] A. Zhu, Y. Tanaka, A. Goldberg, and D. Hong, “Aura: Autonomous upskilling with retrieval-augmented agents,” 2025. [Online]. Available: <https://arxiv.org/abs/2506.02507>
- [9] Y. Li, W. Du, C. Yu, P. Li, Z. Zhao, T. Liu, C. Jiang, Y. Zhu, and S. Huang, “Taccel: Scaling up vision-based tactile robotics via high-performance gpu simulation,” 2025.
- [10] Z. Zhao, H. Dong, Z. He, Y. Li, X. Yi, and Z. Li, “Closing the reality gap: Zero-shot sim-to-real deployment for dexterous force-based grasping and manipulation,” 2026. [Online]. Available: <https://arxiv.org/abs/2601.02778>
- [11] A. Handa, K. Van Wyk, W. Yang, J. Liang *et al.*, “Dexpilot: Vision-based teleoperation of dexterous robotic hand-arm system,” in *IEEE International Conference on Robotics and Automation (ICRA)*, 2020.
- [12] Z. Fu, T. Z. Zhao, and C. Finn, “Mobile aloha: Learning bimanual mobile manipulation with low-cost whole-body teleoperation,” 2024.
- [13] M. Xu, H. Zhang, Y. Hou, Z. Xu, L. Fan, M. Veloso, and S. Song, “Dexumi: Using human hand as the universal manipulation interface for dexterous manipulation,” *arXiv preprint arXiv:2505.21864*, 2025, coRL 2025 Best Paper Finalist.
- [14] H.-S. Fang, B. Romero, Y. Xie, A. Hu, B.-R. Huang, J. Alvarez, M. Kim, G. Margolis, K. Anbarasu, M. Tomizuka, E. Adelson, and P. Agrawal, “Dexop: A device for robotic transfer of dexterous human manipulation,” *arXiv preprint arXiv:2509.04441*, 2025.
- [15] J. Du *et al.*, “Mile: A mechanically isomorphic exoskeleton data collection system with fingertip visuotactile sensing for dexterous manipulation,” 2025.
- [16] R. Ge *et al.*, “Design of a self-aligning four-finger exoskeleton for finger abduction/adduction and flexion/extension motion,” *Biomedical Engineering*, 2023.
- [17] C. Brogi *et al.*, “An original hybrid-architecture finger mechanism for wearable hand exoskeletons: a thumb module study,” *Expert Systems with Applications*, 2024.
- [18] Z. Si *et al.*, “Tilde: Teleoperation for dexterous in-hand manipulation learning with a deltahand,” 2024.
- [19] P. Ruppel *et al.*, “Elastic tactile sensor glove for dexterous teaching by human demonstration,” *Sensors*, vol. 24, no. 6, p. 1912, 2024.
- [20] X. Lin, K. Yao, L. Xu, X. Wang, X. Li, Y. Wang, and M. Li, “Dexflow: A unified approach for dexterous hand pose retargeting and interaction,” 2025. [Online]. Available: <https://arxiv.org/abs/2505.01083>
- [21] Z. Mandi *et al.*, “Functional retargeting for bimanual dexterous manipulation,” 2025.
- [22] Z.-H. Yin, C. Wang, L. Pineda, K. Bodduluri, T. Wu, P. Abbeel, and M. Mukadam, “Geometric retargeting: A principled, ultrafast neural hand retargeting algorithm,” 2025. [Online]. Available: <https://arxiv.org/abs/2503.07541>
- [23] J. Hsieh, K.-H. Tu, K.-H. Hung, and T.-W. Ke, “Dexman: Learning bimanual dexterous manipulation from human and generated videos,” 2025. [Online]. Available: <https://arxiv.org/abs/2510.08475>
- [24] T. Chen *et al.*, “Visual dexterity: In-hand reorientation of novel and complex object shapes,” *Science Robotics*, 2023.
- [25] P. Koczy, M. C. Welle, and D. Kragic, “Learning dexterous in-hand manipulation with multifingered hands via visuomotor diffusion,” 2025. [Online]. Available: <https://arxiv.org/abs/2503.02587>
- [26] Q. Liu *et al.*, “Vtdexmanip: A dataset and benchmark for visual-tactile pretraining and dexterous manipulation,” in *International Conference on Learning Representations (ICLR)*, 2025.
- [27] X. Wang *et al.*, “Medical imaging-based kinematic modeling for biomimetic hand rehabilitation exoskeletons,” *Robotics and Biomechanics*, 2025.
- [28] X. Chi, C. Zhang, Y. Su, L. Dou, F. Yang, J. Zhao, H. Zhou, X. Jia, Y. Zhou, and S. An, “Open teledex: A hardware-agnostic teleoperation system for imitation learning based dexterous manipulation,” 2025. [Online]. Available: <https://arxiv.org/abs/2510.14771>